Astronomy & Astrophysics manuscript no.
(will be inserted by hand later)

XMM−Newton observations of Markarian 421*

W. Brinkmann[1], S. Sembay[2], R. G. Griffiths[2], G. Branduardi-Raymont[3], M. Gliozzi[1], Th. Boller[1], A. Tiengo[4], S. Molendi[5], and S. Zane[3]

[1] Max–Planck–Institut für extraterrestrische Physik, Giessenbachstrasse, D-85740 Garching, Germany
[2] X-ray Astronomy Group, Department of Physics and Astronomy, University of Leicester, LE1 7RH, U.K.
[3] Mullard Space Science Laboratory, University College London, Holmbury St Mary, Dorking, Surrey, RH5 6NT, U.K.
[4] XMM-Newton Science Operation Centre, Villafranca Satellite Tracking Station, 28080 Madrid, ES
[5] Istituto di Fisica Cosmica "G.Occhialini", Via Bassini 15, I-20133, Italy

Received ? / Accepted ?

Abstract. The BL Lac object Mrk 421 was observed on May 25, 2000 during the XMM−Newton Cal/PV phase. The high throughput of the X-ray telescopes and the spectral capabilities of the instruments allow an uninterrupted temporal and spectral study of the source with unprecedented time resolution.
Mrk 421 was found at a relatively high state with a 2−6 keV flux of $(1.3 - 1.9) \times 10^{-10}$ erg cm^{-2} s^{-1}. The observed intensity variations by more than a factor of three at highest X-ray energies are accompanied by complex spectral variations with only a small time lag ($\tau = 265^{+116}_{-102}$ seconds) between the hard and soft photons.
The (0.2−10) keV spectrum can be well fitted by a broken power law and no absorption structures are found in the source spectrum at the high spectral resolution of the transmission gratings.

Key words. BL Lac objects — general; Galaxies: active – quasars; X–rays: general – Radio sources: general.

1. INTRODUCTION

Mrk 421 is the brightest BL Lac object at X-ray and UV wavelengths and it is the first extragalactic source discovered at TeV energies (Punch et al. 1992). This nearby ($z = 0.031$) X-ray bright BL Lac has been observed by essentially all previous X-ray missions and shows remarkable X-ray variability correlated with strong activity at TeV energies (e.g., Takahashi et al. 1996, Maraschi et al. 1999).

BL Lacs are thought to be dominated by relativistic jets seen at small angles to the line of sight (Urry & Padovani 1995), and their radio-through-X-ray spectra are well fitted by inhomogeneous jet models (Bregman et al. 1987). However, the structure of the relativistic jets remains largely unknown as the models are generally under-constrained by single epoch spectra and the typical smooth and nearly featureless blazar spectra can be reproduced by models with widely different assumptions (e.g., Königl 1989).

Combining spectral and temporal information greatly constrains the jet physics. Time scales are related to the crossing times of the emission regions which depend on wavelength and/or the time scales of micro-physical processes like acceleration and radiative losses. The measured lags between the light curves at different energies as well as spectral changes during intensity variations allow to probe the micro-physics of particle acceleration and radiation in the jet. Thus XMM−Newton with its high sensitivity and broad energy bandwidth is an ideal tool to study BL Lacs as it allows spectroscopy with unprecedented time resolution, uninterrupted by gaps because of the long period of the satellite orbit.

Mrk 421 was the first BL Lac object to be established as an X-ray source (Ricketts et al. 1976, Cooke et al. 1978) and subsequent observations indicated that the X-ray spectrum has a soft power law form (Mushotzky et al. 1978, Hall et al. 1981) which exhibits significant variability (Mushotzky et al. 1979). More detailed studies with IUE and EXOSAT showed that the variability occurs on time scales of typically a day with an e-folding time scale of $\sim 5 \times 10^4$ s (George et al. 1988). The source shows a dichotomy of X-ray states: a low, soft state ($f_{2-6\mathrm{keV}} \lesssim 2 \times 10^{-11}$ erg cm^{-2} s^{-1}, $\Gamma \sim 2.8$) where the source hardens when it brightens and a hard outburst state ($f_{2-6\mathrm{keV}} \gtrsim 8 \times 10^{-11}$ erg cm^{-2} s^{-1}) during which the spectral index remains at $\Gamma \sim 2$.

In several Ginga observations, partly simultaneously with ROSAT, Mrk 421 was found at intermediate fluxes of $f_{2-6\ \mathrm{keV}} = (3.6 - 5.2) \times 10^{-11}$ erg cm^{-2} s^{-1} (Makino et al. 1992, Tashiro 1994). The data indicated that the amplitude of the flux variations with time

Send offprint requests to: W. Brinkmann, e-mail: wpb@mpe.mpg.de

* Based on observations with XMM−Newton, an ESA Science Mission with instruments and contributions directly funded by ESA Member States and the USA (NASA)

scales of a few hours got larger with increasing energy and the correlation between flux and spectral index was inconsistent with that observed by EXOSAT. The quality of the spectral fits improved considerably by using a broken power law or a power law with exponential cut off and the Ginga spectrum was significantly steeper than the simultaneous ROSAT spectrum.

Since its discovery as a TeV source several multi-wavelength campaigns have been conducted to study possible time lags between the X-ray band and TeV energies and to investigate the pronounced spectral evolution during flares seen in X-rays with ASCA and BeppoSAX (Macomb et al. 1995, 1996, Takahashi et al. 1996, Fossati et al. 1998, Maraschi et al. 1999). The source generally shows a complex behavior. While Takahashi et al. (1996) found a lag of about 4000 seconds between the soft (0.5 - 1.0 keV) photons and the hard band (2 - 7.5 keV), which was interpreted as an effect of radiative cooling, recent ASCA observations show both, positive and negative lags (Takahashi et al. 2000). BeppoSAX observations of a flare in April 1998, simultaneously observed at TeV energies, showed that the hard photons lag the soft ones by 2-3 ksec and that, while the light curve is symmetric at softest X-ray energies, it becomes increasingly asymmetric at higher energies with the decay being slower than the rise (Fossati et al. 2000).

Fitting the ASCA data by a simple power law Takahashi et al. (1996) find that an absorbing column density considerably higher than the Galactic value of $N_H = 1.5 \times 10^{20}$ cm^{-2} (Elvis et al. 1989) is required to obtain acceptable fits. Fixing the absorption at the Galactic value a broken power law model provides a better fit than a simple power law, but the $\chi^2_{\rm red}$ is often un-acceptable. With these models the break energy is at $\sim$ 1.5 keV, and the change of the power law index at the break point is $\Delta\Gamma \sim 0.5$.

With the wider energy range of BeppoSAX it became clear that these simple models are not adequate descriptions of the downward curved Synchrotron spectra (Fossati et al. 2000) and continuously curved shapes had to be employed (Inoue & Takahara 1996, Tavecchio et al. 1998). The Synchrotron peak energy varied between 0.4− 1 keV, the spectral index at an energy of 5 keV between $1.5 \leq \alpha \leq 2.2$. Both quantities are correlated with the X-ray flux: the peak energy positively, the spectral slope inversely: with increasing flux the synchrotron peak shifts to higher energies and the spectrum at 5 keV gets flatter.

Most of these results were obtained from data integrated over wide time intervals (typically one satellite orbit) and from giant flares with time scales of a day. Uninterrupted data with high temporal and spectral resolution can only be provided by XMM−Newton with its high sensitivity, spectral resolving power, and broad energy band.

2. XMM−Newton observations

Mrk 421 was observed with the European Photon Imaging Camera (EPIC) and the RGS during orbit 84 (May 25, 2000) of the calibration and performance verification phase (Cal/PV) of XMM−Newton. The EPIC-PN camera was first operated from UT 3:53 - UT 10:11 in the fast timing mode, then, from UT 11:34 to UT 19:34, in Small Window (SW) mode. As the data analysis tools for the timing mode are not yet fully established we will restrict our discussion mainly to the second part of the observation, where the PN camera was operated in the SW mode. This mode, with a frame integration time of $\sim$ 5.7 msec was chosen to avoid photon pile-up in this strong source. Overall, a total of more than 8.9 million counts were accumulated in SW mode in a net observation time of $\lesssim$ 33 ksec, predominantly originating from the source itself.

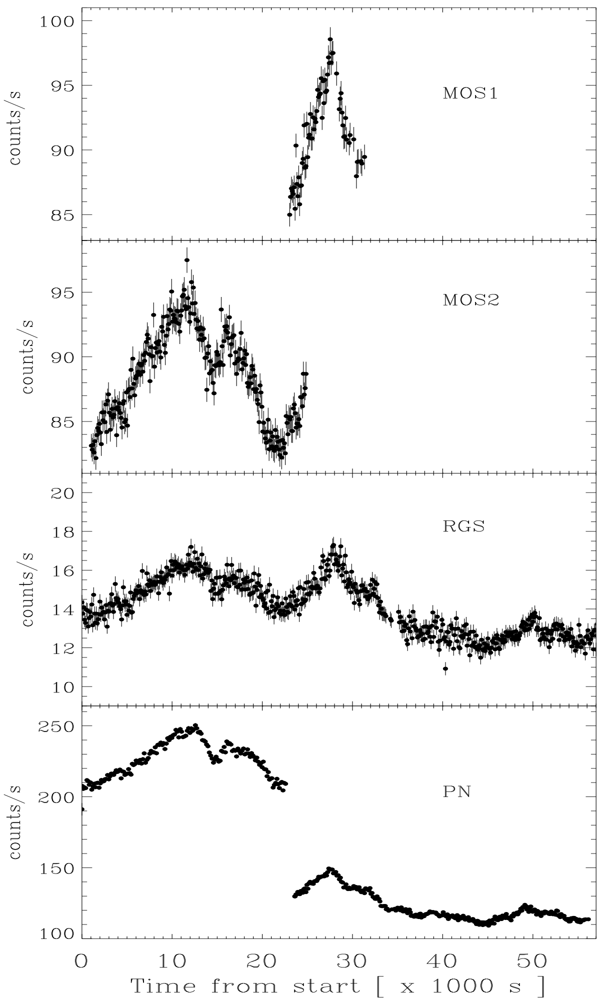

Fig. 1. Light curves of Mrk 421 during the XMM−Newton observation in the different instruments.

Two separate observations of Mrk 421 were performed with the MOS cameras, one in timing mode and the other in partial window mode with a free running readout (PRI PART W4). During both observations the medium filter was selected. For the purposes of this paper, however, only data taken in partial window mode is used. In PRI PART W4 mode only a fraction of the central chip (100 x 100 pixels) is read out giving a time resolution of 0.2 s. Exposure times of 7 ksec and 24 ksec were obtained by MOS1 and MOS2 respectively. A standard reduction of raw MOS event lists was performed, using the XMM−Newton Science Analysis System (SAS) and only 'real' X-ray events with a pattern 0-12 were used to create spectra and light curves for further analysis.

MOS data and PN imaging data only have a small overlap in time. Due to a radiation alert the MOS cameras were switched off shortly after the PN SW mode observation began and were not turned on again. So the ∼30 ksec of available MOS time largely precedes the PN observation; the actual overlap is only about 5 ksec.

Both RGS instrument chains also observed Mrk 421 in two exposures for a total observing time of 64 ksec; thus the RGS coverage is slightly longer than that of EPIC. The data were acquired in the RGS standard spectroscopy mode, where the full spectrum is read-out every ∼ 6 s (for details on the RGS instrument see den Herder et al., this volume). The data were processed with the SAS, using the most up-to-date calibration parameters.

Fig. 1 shows the light curves of the whole observation for the different instruments. The count rate plots provide only a qualitative picture as the photons in the individual instruments are selected according to different criteria, neither covering the same energy ranges nor originating from identical spatial regions around the source. This is most clearly seen in the PN data taken in Fast Timing and in Small Window mode, which do not match in count rate when the modes were changed. The quantitatively correct conversion from count rates to fluxes is detector and operation mode dependent and must be deferred to a later paper.

No scientific data are available from the Optical Monitor for this observation of Mrk 421.

2.1. PN light curves

Light curves were produced by using the PN photon event files produced by the SAS. Only single events with energies 0.2 keV $\lesssim$ E $\lesssim$ 10 keV were selected from a circle of 9 detector pixels radius (corresponding to $\sim 38''$) around the source center; the background was taken from the outer source-free region of the detector and amounted to about 3% of the source counts.

The photons were first binned into 10 sec intervals which turned out to be necessary as the accepted time intervals are frequently disrupted by short gaps where the camera fell into counting mode. Finally, the binned data were summed up into typically 100 s bins providing an excellent signal to noise ratio.

Fig. 2 shows the background subtracted light curves in three energy intervals: the total 0.2-10 keV count rate at the top, then the soft (E $\leq$ 1 keV) and the hard (E $>$ 3 keV) light curves in the middle, all in 100 s time bins and, at the bottom, the hardness ratios of the count rates in the $(3-10\,\mathrm{keV})/(0.2-1\,\mathrm{keV})$ bands.

The total light curve shows intensity variations of about a factor of 1.5; at high energies the maximal variation is much stronger, about a factor of 3.4 during the SW mode exposure. The source gets harder when it flares, in accordance to previous observations. The hard flux is considerably more variable than the soft flux as quantified by the excess variance (Nandra et al. 1997): for the soft band it is $(4.29 \pm 0.01) \cdot 10^{-3}$ while for the hard band it is $(2.45 \pm 0.05) \cdot 10^{-2}$.

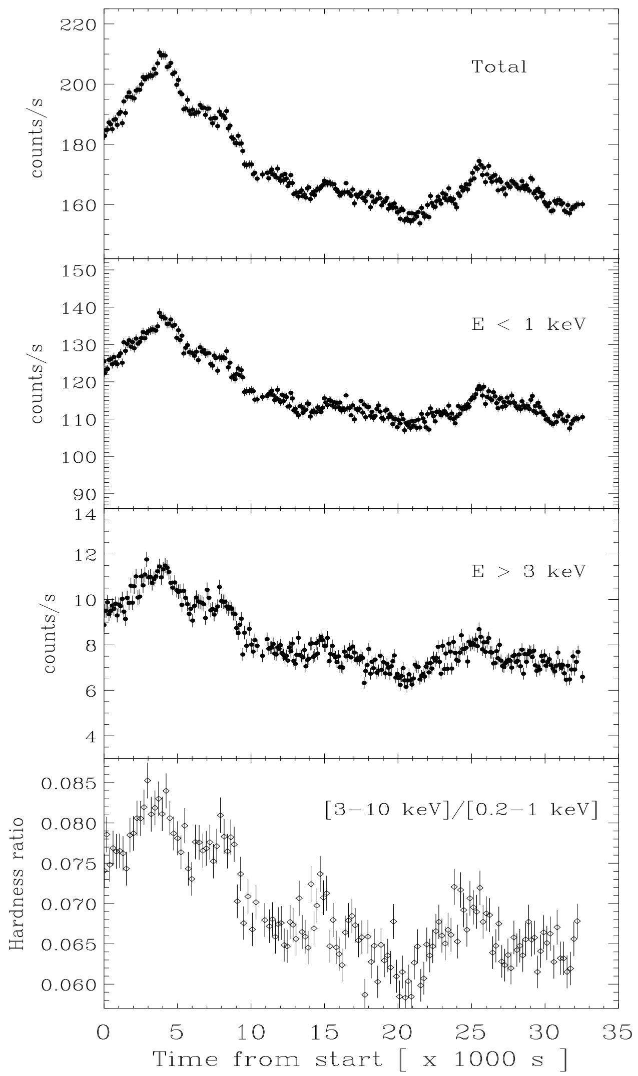

Fig. 2. The EPIC PN light curve of Mrk 421 during orbit 84. The time is counted from the start of the SW mode observation. Only single events were taken and a time binning of 100 seconds has been used. Shown from the top are: the total 0.2-10 keV count rate ; the count rate for the soft photons E$\leq$ 1 keV, for the hard photons E $>$ 3 keV, and at the bottom the hardness ratio between the hard and the soft photons.

The source was found in a relatively high state. From the spectral fit to the total data set (see Sect. 3) we obtain an average $2-6$ keV flux of $(1.3-1.9)\times 10^{-10}$ erg cm^{-2} s^{-1} which is considerably higher than the 'classical' soft state, but still lower than in the April 1998 observation of BeppoSAX (Fossati et al. 2000).

The light curve is rather complex and seems to consist of several, partly overlapping flares on top of smooth intensity variations. The spectral evolution during the two prominent flares at ∼ 3 ksec and ∼ 25 ksec after the start of the observation shows a clockwise hysteresis, as seen in Fig. 3. This effect was already noted in previous ASCA observations (Takahashi et al. 1996) but as a property of the long term (∼ 1 day) intensity variations of the source.

The flares seem to have nearly linear rise- and decay profiles which are asymmetric with energy dependent time scales.

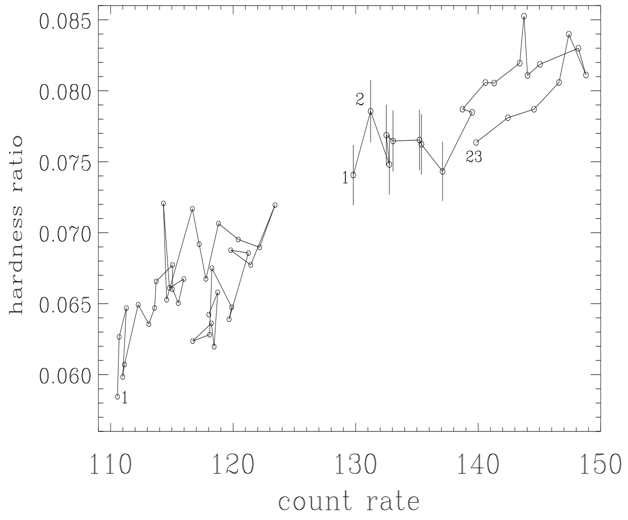

Fig. 3. Spectral evolution during the two prominent flares occuring at $\sim$ 3 ksec and $\sim$ 25 ksec after the start of the observation. Plotted are the hardness ratios as function of total count rate and a few error bars at the beginning of the first peak. Numbers indicate the temporal sequences of the data.

In the total band the first flare rises slower ($\sim$ 4.7×10^{-3} counts s^{-2}) than it decays ($\sim$ 8.8×10^{-3} counts s^{-2}), but in general an exact determination of these time scales is problematic due to the occurrence of additional, overlapping smaller flares. In Fig. 3 these lead to a break of the clean intensity - hardness ratio correlation at the end of the decaying part of the flares.

The flare profiles are energy dependent and we quantified the time delays between the hard and soft photons employing the Z-transformed discrete cross-correlation function algorithm (ZDCF) of Alexander (1997). The soft photons lag the hard by 265^{+116}_{-102} seconds where the 1σ errors were determined by using a Monte Carlo method described by Peterson et al. (1998). Lags of a few 1000 secs as claimed from previous observations (Takahashi et al. 1996, Fossati et al. 2000) must thus be related to long-term flux changes and not to individual flares.

2.2. Structure function analysis

A structure function analysis is a method of quantifying time variability without the problems encountered in the traditional Fourier analysis technique in case of unevenly sampled data. The first-order structure function (Simonetti et al. 1985) measures the mean deviation for data points separated by a time lag τ, $SF(\tau) = \langle[F(t) - F(t+\tau)]^2\rangle$. It is commonly characterized in terms of its slope: $b = d\log(SF)/d\log\tau$. One of the most useful features of the structure function is its ability to discern the range of time scales that contribute to the variations in the data set. For lags shorter than the smallest correlation time scale and for lags longer than the longest correlation time scale, the structure function displays two plateau states ($b = 0$) at different levels. These regions are linked by a curve whose slope depends on the nature of the intrinsic variation of the source (e.g. flicker noise, shot noise, etc.).

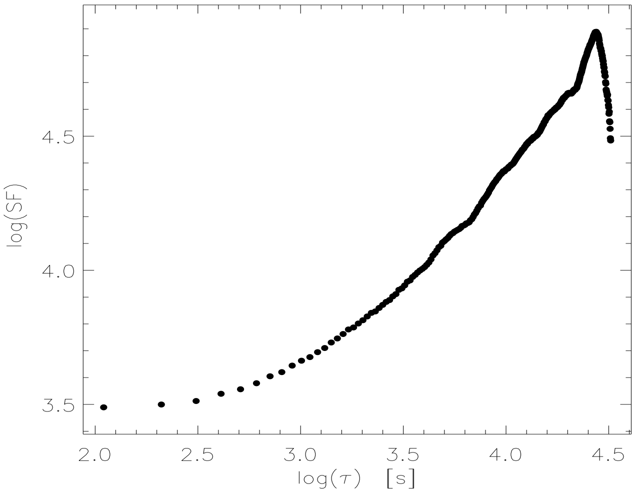

Fig. 4. Structure function of Mrk 421. Time lags are in secs.

Fig. 4 shows the structure function of Mrk 421 obtained from single events during the SW mode observation. The 'wavy' structure of the increasing part must be related to the few individual flares in the light curve. Mrk 421 shows little variation at time scales lower than 10^3 s. For longer time scales the slope of the structure function is $b \sim 1$ which indicates that the nature of the variation of the source can be ascribed to shot noise. The current data do not allow to see the roll-over at a lag of about half a day, found by ASCA (Takahashi et al. 2000). The result is fully consistent with the findings of Hughes et al. (1992), who obtained an average slope of 0.94 ± 0.37 for a sample of 20 BL Lac objects.

3. Spectral analysis

The X-ray spectrum of Mrk 421 was repeatedly studied in the past and fitted to a featureless power law or broken power law. By taking the single events from the whole PN SW mode data set, employing the latest versions of the detector response and CTE corrections, we find that a power law with frozen Galactic absorption does not fit the 0.2-10 keV data (χ^2_{red} = 2.025), while the fit improves leaving the absorption column density free ($N_H = (3.05 \pm 0.07) \times 10^{20}$ cm^{-2}, $\Gamma = 2.41 \pm 0.06$ at a $\chi^2_{red} = 1.54$ for 1246 d.o.f).

A broken power law with free absorption gives an acceptable fit to the data (see Fig. 5). The best fit parameters are $N_H = (1.66 \pm 1.37) \times 10^{19}$ cm^{-2}, $\Gamma_1 = 1.448 \pm 0.054$, E$_{break}$ = (0.584 ± 0.007) keV, $\Gamma_2 = 2.329 \pm 0.007$ at a $\chi^2_{red} = 1.16$ for 1244 d.o.f. There are still systematic (instrumental) deviations in the residuals at low energies around 0.3 keV and 0.5 keV, as clearly visible in Fig. 5, leading to an inexact determination of the absorption column density. Note the extremely high statistical significance in the data: at lower energies every spectral bin contains more than 2000 counts!

With these spectral parameters the source average flux in the 2−6 keV bands amounts to $(1.3 - 1.9) \times 10^{-10}$ erg cm^{-2} s^{-1}, where the quoted uncertainty originates mainly from the currently uncertain contributions of the double, triple, and unrecognized events to the 'real' source flux.

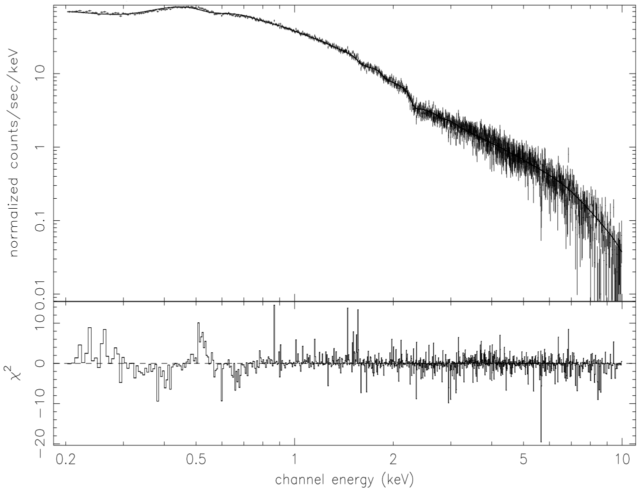

Fig. 5. Broken power law fit to the total PN Small Window mode data of Mrk 421. Only single events were used.

In the RGS spatial and spectral domains (i.e. in the dispersion vs cross-dispersion, and dispersion vs CCD pulse height, event distributions) data cuts were made in order to extract the source spectra in both first and second order. Spectra of the background (which is $\sim$ 1% of the source flux) were extracted from a spatial region offset from the source in the cross dispersion direction, and as wide as that used for the source. Instrumental responses were built for first and second order spectra for RGS1 and RGS2 (in 3000 spectral bins).

The model that best fits the Mrk 421 RGS data is a broken power law; other models were tried (but no 'curved' models), but none matched the data better. The RGS1 first order spectra for the two exposures were fitted simultaneously with the same absorbed broken power law model, keeping all parameters tied, except for the normalizations which were allowed to vary independently; the low-energy absorption column density was fixed at the Galactic value. The best fit parameters are $\Gamma_1 = 1.76 \pm 0.01$, $\Gamma_2 = 1.94 \pm 0.01$, $E_{break} = 0.89^{+0.04}_{-0.03}$ and a reduced χ^2_{red} = 1.68.

Data from the second RGS1 exposure (strictly simultaneous with the spectra obtained from the PN camera) were analyzed on their own, with similar results to the total dataset. Further, we find no evidence for any discrete spectral feature (neither in absorption, nor in emission) in the Mrk 421 data. The RGS spectra allow us to set a 90% upper limit of 0.3 eV (0.012 Å) to the EW of a narrow, saturated OVII resonance absorption line at 0.574 keV (21.6 Å; these values correspond to 0.557 keV, and 22.3 Å, respectively, at the redshift of the galaxy). The presence of such an absorption feature was was suggested by Guainazzi et al. (1999) from BeppoSAX observations. A similar RGS upper limit applies to the EW of an OVIII Lα resonant absorption line at 0.654 keV.

3.1. Spectral comparison

The flare at the beginning of the SW mode observation was observed by the MOS1 camera as well and could thus be fit with both, the PN and the MOS instruments.

A broken power law model with the absorption fixed at the Galactic value resulted for the MOS1 in an acceptable fit (χ^2_{red} = 1.04 for 213 d.o.f.) with: $\Gamma_1 = 2.004 \pm 0.004$, $\Gamma_2 = 2.295 \pm 0.078$, $E_{break} = 2.33 \pm 0.08$ keV. The same model (fixed Galactic absorption and broken power law) did not yield an acceptable fit in the PN; only when the N_H - value was left as a free parameter we obtained acceptable fits with $\chi^2_{red} \sim 1.0$. While the fitted slope of the high energy power law remained stable ($\Gamma_2 = 2.33 \pm 0.03$) and nearly identical to the MOS1 value in all fits, the other parameters depended strongly on the actual lower boundary of the energy range for the fit. The fitted N_H always remains lower than the Galactic value.

Similarly, broken power law fits at different intensity levels of Mrk 421 tend to yield nearly identical slopes at higher energies, only the low energy slopes and the break energies seem to vary. In conclusion, the above fit comparisons indicate that the cross calibration of the spectral responses still needs improving.

4. Summary

X-ray observations have been used frequently to determine the physical conditions of the central engines of BL Lac objects. In most cases integration times over typically one satellite orbit inhibited the study of irregularities in the variability patterns and the puzzling spectral behavior of the sources on shorter time scales. XMM−Newton with its high sensitivity and broad energy bandwidth allows spectroscopy with unprecedented time resolution, uninterrupted by gaps because of the long period of the satellite orbit.

In the extended XMM−Newton Cal/PV observations of Mrk 421 in May 25, 2000 the source was found in a relatively high state with intensity variations by a factor of more than 3. In the hard energy band the source is considerably more variable than in the soft band, but in the time resolved flares we find only a small time lag between the hard and the soft photons. This result and the fact that the shape of individual pulses and their spectral evolution are resolvable on time scales of $\sim$ 100 secs, puts strong constraints on time dependent radiation models for BL Lac jets (Georganopoulos & Marscher 1997, Kirk et al. 1998,Chiaberge & Ghisellini 1999, Kataoka et al. 1999).

The spectra can be well fitted by broken power laws with break energies around 1−2 keV. Flux variations seem to affect the low energy power law slope and the value of the break energy; the higher energy slope appears to be quite stable. A quantitative analysis, however, will have to await a further reduction of the remaining calibration uncertainties.

Acknowledgements. We thank I. Papadakis for his help with the cross-correlation analysis and K. Dennerl, S. Zavlin, and F. Haberl for producing off-line event files with currently unpublished CTE corrections. The XMM−Newton project is supported by the Bundesministerium fuer Bildung und Forschung / Deutsches Zentrum fuer Luft- und Raumfahrt (BMBF/DLR), the Max-Planck Society and the Heidenhain-Stiftung. The Mullard Space Science Laboratory and Leicester University acknowledge financial support from the UK Particle Physics and Astronomy Research Council. Part of this work was done in the TMR research network 'Accretion onto black holes, compact stars and protostars' funded by the European Commission under contract number ERBFMRX-CT98-0195.

References

Alexander T., 1997, in: Astronomical Time Series, ed. D. Maoz, A. Sternberg, E.M. Leibowitz, Dordrecht, Kluwer, p.163

Bregman, J., Maraschi, L., Urry, C.M. 1987, in *Exploring the Universe with the IUE Satellite*, ed. Y. Kondo (Dordrecht: Reidel), p. 685

Chiaberge M., Ghisellini G., 1999, MNRAS 306, 551

Cooke B.A., Ricketts M.J., Maccacaro T., et al., 1978, Mon. Not. R. astr. Soc. 182, 489

Elvis M., Lockman F.J., Wilkes B.J., 1989, AJ 97, 777

Fossati G., Chiappetti L, Celotti A., et al., 1998, Nucl. Phys. B. Proc. Supp. 69/1-3, 423

Fossati G., Celotti A., Chiaberge M., et al., 2000, astro-ph/0005066, astro-ph/0005067

Georganopoulos M., Marscher A.P., 1997, in: *Relativistic Jets in AGN*, eds M. Ostrowski et al. , Krakow, Poland, p. 313

George I.M., Warwick R.S., Bromage G.E., 1988, Mon. Not. R. astr. Soc. 232, 793

Guainazzi M., Vacanti G., Malizia A., et al., 1999, A&A 342, 124

Hall R., Ricketts M.J., Page C., Pounds K.A., 1981, Space Sci. Rev. 30, 47

Hughes P.A., Aller H.D., Aller M.F., 1992, ApJ 396, 469

Inoue S., Takahara F., 1996, ApJ 463, 555

Kataoka J., Takahashi T., Makino F., et al. , 1999, ISAS Research Note 687

Kirk J.G., Rieger F.M., Mastichiades A., 1998, A&A 333, 452

Königl, A. 1989, in: BL Lac Objects, ed. L. Maraschi, T. Maccacaro, & M.-H. Ulrich, (Berlin: Springer-Verlag), p. 321

Macomb D.J., Akerlof C.W., Aller D.H., et al., 1995, ApJ 449, L99

Macomb D.J., Akerlof C.W., Aller D.H., et al., 1996, ApJ 459, L111

Makino F., Fink H.H., Clavel J., 1992, in: Frontiers of X-ray Astronomy, eds. Y. Tanaka, K. Koyama (Tokyo: Univ. Acad. Press), p. 543

Maraschi L., Fossati G., Tavecchio F., et al., 1999, ApJ 526, L81

Mushotzky R.F., Boldt E.A., Holt S.S., et al., 1978, ApJ 226, L65

Mushotzky R.F., Boldt E.A., Holt S.S., Serlemitsos P.J., 1979, ApJ 232, L17

Nandra K., George I.M., Mushotzky R.F., Turner T.J., Yakoob T., 1997, ApJ 476, 70

Peterson B.M., Wanders I., Horne K., et al., 1998, Pub. Astr. Soc. Pac. 110, 660

Punch M., Akerlof C.W., Cawley M.F., et al., 1992, Nature 358, 477

Ricketts M.J., Cooke B.A., Pounds K.A., 1976, Nature 259, 546

Simonetti J.H., Cordes M.J., Heeschen D.S., 1985, ApJ 296, 46

Takahashi T., Tashiro M., Madejski G., et al. , 1996, ApJ 470, L89

Takahashi T., Kataoka J., Madejski G., et al., 2000, astro-ph/0008505

Tashiro M., 1994, PhD thesis, Univ. of Tokyo; ISAS Research Note 549

Tavecchio F., Maraschi L., Ghisellini G, 1998, ApJ 509, 608

Urry, C.M., & Padovani, P. 1995, PASP, 107, 803